Microchemical Journal 179 (2022) 107441

Contents lists available at ScienceDirect

Microchemical Journal

journal homepage: www.elsevier.com/locate/microc

A shipboard method for catalytic kinetic spectrophotometric determination of trace Cu(II) concentrations in seawater using reverse flow injection analysis coupled with a long path length liquid waveguide capillary cell

Ting Wang [a,b], Yongming Huang [a], Yong Zhu [c], Jin Xu [a], Dewang Li [c], Bin Wang [c], Weidong Guo [a,b,*], Dongxing Yuan [a,*]

[a] State Key Laboratory of Marine Environmental Science, Xiamen University, Xiamen, China
[b] College of Ocean and Earth Sciences, Xiamen University, Xiamen, China
[c] Key Laboratory of Marine Ecosystem Dynamics, Second Institute of Oceanography, Ministry of Natural Resources, Hangzhou, China

ARTICLE INFO

Keywords:
Cu(II)
Catalytic kinetic method
Spectrophotometry
Reverse flow injection analysis
Liquid waveguide capillary cell
Estuarine and coastal waters

ABSTRACT

By using reverse flow injection analysis (rFIA) and a 1.0 m liquid waveguide capillary cell (LWCC), an automatic and sensitive catalytic kinetic spectrophotometric method for on-line monitoring of Cu(II) concentrations in estuarine and coastal waters was established. Cu(II) detection was based on its catalytic effect on glutathione (GSH) oxidation by potassium ferricyanide under acidic conditions. The change in absorbance of potassium ferricyanide at 420 nm was used to monitor the reaction spectrophotometrically. Experimental parameters were optimized using a univariate experimental design approach and it was ensured that the method was free of interference from co-occurring ions such as Fe(II), Fe(III), Mn, Zn, Cd, Al, Cr, Ni and Co. The proposed method was shown to have high sensitivity with a detection limit of 0.15 nmol L^{-1} in a pure water matrix and 0.23 nmol L^{-1} in a seawater matrix. Linearity was achieved within the range of 0.45–15 nmol L^{-1} in a pure water matrix and 0.69–10 nmol L^{-1} in a seawater matrix using a 200 cm reaction coil, while the upper limits can be extended to 40 and 25 nmol L^{-1}, respectively, by using a shorter (100 cm) reaction coil. A high level of Cu(II) recovery was maintained, ranging between 95.2% and 101%. The relative standard deviations (RSDs) of blanks and samples spiked with 5 nmol L^{-1} Cu(II) standard were 1.52% (n = 13) and 1.10% (n = 13), respectively. The method was confirmed to be free of carry-over effect and a sample throughput of 26 h^{-1} was achieved. The method was successfully applied to underway and on-board determination of Cu(II) concentrations from a surface transect in the Jiulong Estuary and a vertical profile in the Yangtze Estuary, China, respectively.

1. Introduction

As one of the most important essential trace metals in the marine ecosystem, copper (Cu) is required by various enzymes involved in electron transport [1] and plays a co-limiting role (together with iron) in the growth and distribution of pelagic phytoplankton [2]. In oxidized seawater environments, Cu mainly exists in the form of Cu(II), accounting for 90–95% of the total dissolved Cu concentration [3]. Nevertheless, Cu(II) is toxic to phytoplankton at high concentrations (>93.8 nmol L^{-1}) since its ability to form strong complexes with biomolecules [4–7]. As the marine environment is a dynamic system that exhibits a high level of spatial and temporal variability in Cu(II) distribution [8], developing methods for high-frequency real-time or on-board determination of Cu(II) concentrations will be a great advantage, helping to reveal its biogeochemical cycles and environmental effects in oceanic environments.

Several methods for the determination of Cu(II) concentrations in seawater have been reported, including inductively coupled plasma-atomic emission spectrometry (ICP-AES) [13], inductively coupled plasma-mass spectrometry (ICP-MS) [14,15], atomic absorption spectrometry (AAS) [9–12], chemiluminescence [16–19] and spectrophotometry [20–25]. To date, ICP-AES, ICP-MS and AAS have been the most commonly adopted methods in marine science studies, as they have high sensitivity and good selectivity. However, these methods all require some form of sample pretreatment, as well as a dedicated laboratory, a stable power supply, ventilation equipment and a cooling system [26].

* Corresponding authors.
E-mail addresses: wdguo@xmu.edu.cn (W. Guo), yuandx@xmu.edu.cn (D. Yuan).

https://doi.org/10.1016/j.microc.2022.107441
Received 16 November 2021; Received in revised form 23 March 2022; Accepted 28 March 2022
Available online 1 April 2022

Chemiluminescence methods have been extensively applied to the analysis of Cu(II) due to their low detection limit, simple operational procedures and low-cost instrumentation. However, chemiluminescence is susceptible to interference from the seawater matrix [16]. The diethyldithiocarbamate (DDTC) spectrophotometric method is low-cost and exhibits good selectivity, although its application has been hindered by low sensitivity, labor-intensive operational procedures and the high toxicity of reagents [24,27]. Compared to the DDTC method, catalytic kinetic analytical methods have the advantages of high sensitivity, simple operational procedures, low analytical costs and low reagent toxicity. Catalytic kinetic methods are based on the catalytic effect of Cu (II) on the reduction of potassium ferricyanide by glutathione (GSH) under acidic conditions. However, the currently available catalytic kinetic spectrophotometric methods require complicated traditional off-line operational steps, using experimental conditions which are hard to control [20,21,25].

The flow analysis technique is a widely used form of automatic analysis, due to its advantages of simple operational procedures, good reproducibility, high degree of automation and low secondary pollution risks [28,29]. The normal flow injection analysis (nFIA) involves injection of a small amount of sample into a closed and continuous flow stream of reagent or carrier, while in reverse FIA (rFIA), the reagent is injected into a flowing sample stream [30]. With rFIA, less reagent is consumed and sample dispersion is at a lower level. Therefore, rFIA is more sensitive than nFIA [31,32]. Additionally, since the sample is used as the flow carrier, rFIA does not require a matrix match and is not affected by either the Schlieren effect [33] or salinity.

Solid phase extraction (SPE) and liquid waveguide capillary cell (LWCC) are the most commonly applied and effective techniques for the determination of trace analytes in flow analysis. Combining FIA with SPE or LWCC and a detection method provides an effective technique for determining trace analytes in field or *in-situ* [34–39]. For Cu(II) analysis, combinations of SPE extraction and various detection methods, have been developed and applied to various aquatic environments [13,40]. However, application of the SPE pretreatment technique has been limited due to the large sample consumption requirements, long analytical duration and short lifetime of SPE cartridges. In comparison to SPE technique, LWCC offers significant time saving, as well as lower levels of sample and reagent consumption [23].

The study developed a rFIA-LWCC-catalytic kinetic spectrophotometric method to on-board determine Cu(II) in estuarine and coastal waters. The automated and sensitive method has been successfully applied to on-line underway determination of Cu(II) concentrations in surface water of the Jiulong Estuary (China), as well as the on-board analysis of discrete samples collected from a vertical profile of the Yangtze Estuary (China).

2. Experimental

2.1. Reagents and standards

All of the reagents and standards were made with pure water (resistivity of $\geq$ 18.2 MΩ·cm), which was obtained through a water purification system (Millipore Co., US). High-density polyethylene containers (Nalgene, US) were used to store reagent and standards solutions, and washed according to the process described by Achterberg et al. [41] before use.

The 10 mmol L^{-1} potassium ferricyanide ($K_3Fe(CN)_6$) stock solution was prepared by dissolving 0.3292 g of $K_3Fe(CN)_6$ (Shanghai Macklin Biochemical Co., Ltd., China) in 100 mL pure water, with a 0.15 mmol L^{-1} $K_3Fe(CN)_6$ working solution obtained by diluting the $K_3Fe(CN)_6$ stock solution with pure water. A 90 mmol L^{-1} reduced L-glutathione (GSH) stock solution was prepared by dissolving 0.4939 g of GSH (Adamas Reagent Co., Ltd., China) in 100 mL pure water, with a 9 mmol L^{-1} GSH working solution then obtained by diluting the GSH stock solution with pure water. The 2 mol L^{-1} acetic acid-sodium acetate buffer stock solution (HAc-NaAc, pH 4.6) was prepared by mixing 27.2 g NaAc (Merck, Germany) and 11.6 mL HAc (Merck, Germany) with 196 mL pure water. The 0.3 mol L^{-1} HAc-NaAc working solution was then obtained by diluting the HAc-NaAc stock solution with pure water.

Cu(II) working solutions were prepared by diluting a commercial copper atomic absorption standard solution (1000 mg L^{-1}, Sigma-Aldrich, US) with acidified pure water or low copper seawater (LCSW), with details provided in section 3.3. A 0.01 mol L^{-1} HCl (Thermo Fisher Scientific Co., US) solution was prepared from concentrated hydrochloric acid and used to prepare all standard solutions.

2.2. Apparatus and analytical procedures

The configuration of the underway system and real-time detection manifold for Cu(II) is shown in Fig. 1. Cu(II) was determined utilizing a laboratory-made universal flow analysis platform. The analyzer was comprised of two four-channel peristaltic pumps (Baoding Shenchen Peristaltic Pump Co. Ltd., China), a thermostatic water bath (Jintan Shunhua Instrument Co. Ltd., China), a six-port two-position injection valve (IV, Valco Instruments, US) and a 1.0 m LWCC (World Precision Instruments, US) connected to a LED lamp (C513A-MSS-CX0Z0231, CREE, USA) and a STS-VIS spectrometer (350–800 nm, Ocean Optics, US) via fiber optic cables. The peristaltic pumps utilized polyethylene tubes of two different inner diameters, 2.06 mm i.d. and 0.89 mm i.d (Valco Instruments Co. Inc., US). Residual manifold tubes were composed of transparent PTFE with a 0.75 mm i.d. (Cole-Parmer, US).

The underway sampling system was suspended with a towed fish at the end of a boom, at a distance of 3 m from the side of the ship [42]. With a 0.45 μm bursal filter on-line, the surface seawater was filtered and acidified with 0.2 mol L^{-1} HCl to pH 2.0 (Fig. 1a). The acidified sample was introduced to the Cu(II) analyzer via a peristaltic pump. When the IV is set to position A (60 s) (Fig. 1b), the sample, $K_3Fe(CN)_6$ and HAc-NaAc buffer solutions were successively mixed and delivered into the detector, while the GSH solution was added to the reagent loop. The absorbance before the catalytic reaction was measured at a wavelength of 420 nm (labeled as A_0). After switching the IV to position B (80 s), the GSH solution was delivered from the reagent loop by the carrier stream (pure water) and then merged with the sample, $K_3Fe(CN)_6$ and HAc-NaAc buffer solutions to catalyze the fading reaction in the reaction coil. Finally, the mixed solution was passed through the LWCC for detection, with the absorbance measured and labeled as A_t. The absorbance difference (A_R) before (A_0) and after (A_t) the catalyzed reactions was calculated according to Equation (1) as follows:

$$A_R = A_0\text{-}A_t \quad (1).$$

Custom-written C++ software was used to automatically control the pump speed, rotation direction, valve position, and duration of each step. The data collection interface of the Cu(II) detection system is exhibited in the supplementary information (Fig. S1). The LWCC was rinsed with pure water, 1 mol L^{-1} NaOH solution, 1 mol L^{-1} HCl solution, and then pure water in sequence before and after usage, with each washing step lasting for at least 10 min (Fig. 1).

2.3. Field investigation

The system was applied in two field studies. Fig. 2a shows the sampling station in the Yangtze Estuary (Eastern China), during a cruise from the 6th to 12th September 2021. Cu(II) concentrations across a vertical profile at station Q49 (123°6′E, 30°43′N) were obtained on board of research vessel Runjiang I. Discrete seawater samples were collected from 13 various depths at station Q49 using a custom-made continuous profile sampler. Salinity and dissolved oxygen (DO) data were also determined along the profile using a multi-parameter sensor (SBE911/17 plus, Sea-Bird Scientific, US).

Underway measurements were carried out in the Jiulong Estuary

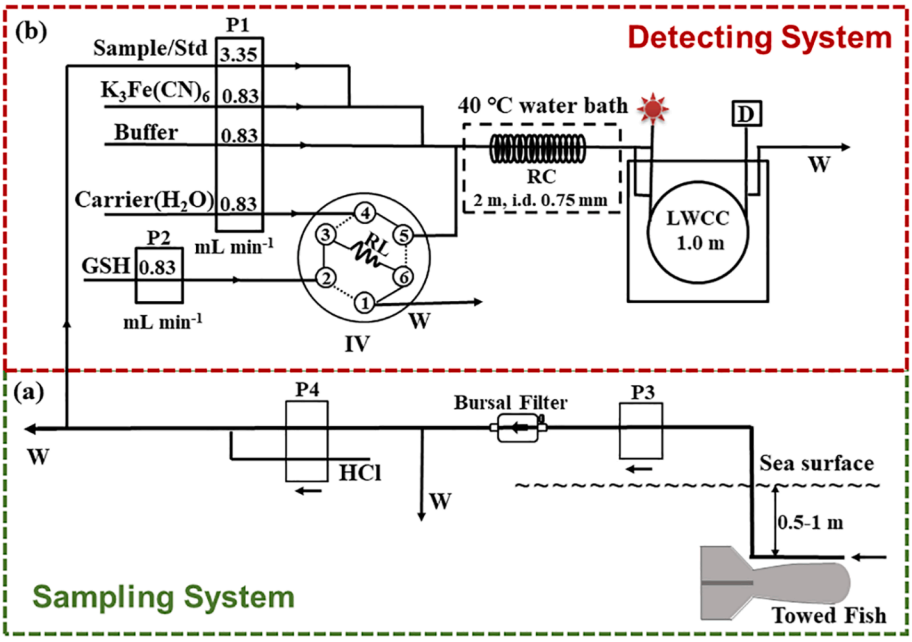

Fig. 1. Configuration of the (a) underway system and (b) real-time detection manifold for Cu(II). P1 and P2: peristaltic pumps, on which the numbers indicate the flow rates (mL min^{-1}); Sample/Std: sample or standards; GSH: glutathione solution; IV: 6-port valve; RL: reagent loop; RC: reaction coil; W: waste. The solid line within the IV represents the valve in position A, while the dashed line represents the valve in position B.

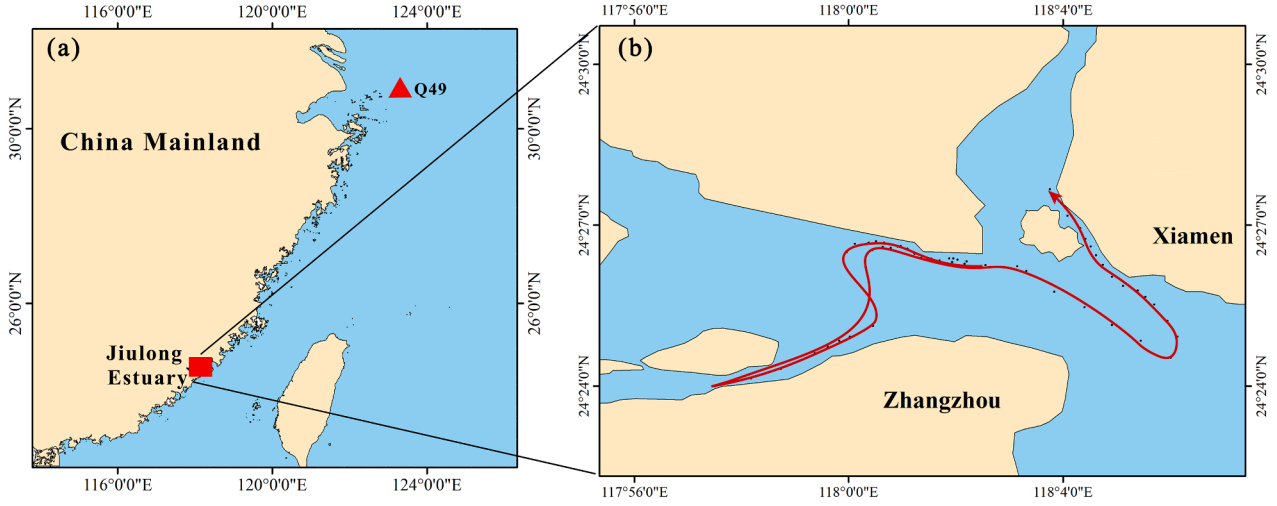

Fig. 2. Map of (a) sampling station Q49 in the Yangtze Estuary (China) and (b) the underway monitoring cruise path (red line) across the Jiulong Estuary (China).

(Southeast China), on-board the Haiyang II research vessel on the 26th June 2021, via the cruise route shown in Fig. 2b. The underway sampling system, continuously pumped water samples into the on-board laboratory using a peristaltic pump, with samples then on-line filtered using a 0.45 μm bursal filter. The filtered sample stream was acidified to pH 2.0 on-line via the addition of 0.2 mol L^{-1} HCl, then transferred to the detection system for analysis (Fig. 2).

3. Results and discussion

3.1. Selection of the detection wavelength

$K_3Fe(CN)_6$ oxidizes GSH under acidic conditions at a very slow speed. However, in the presence of trace concentrations of Cu(II), the reaction is strongly catalyzed. Fig. 3 shows the absorbance spectra of the $K_3Fe(CN)_6$-GSH system in the presence of Cu(II) at different reaction times, showing that the absorbance (A) continuously decreased with increasing reaction time. The $K_3Fe(CN)_6$-GSH system exhibits a maximum absorption peak at a wavelength of 420 nm, and the absorbance difference before and after the reaction, A_R, was the largest. Therefore, 420 nm was selected as the detection wavelength. The color change in the $K_3Fe(CN)_6$-GSH system before and after the catalytic reaction is shown in Fig. S2 (Fig. 3).

3.2. Parameter optimization

Based on a univariate experimental design, the effects of numerous parameters were evaluated and optimized, including the concentrations of $K_3Fe(CN)_6$, GSH and the HAc-NaAc buffer, the HAc-NaAc buffer pH, the reagent injection volume, the reaction coil length and the reaction temperature. A blank and a 20 nmol L^{-1} Cu(II) standard solution in a pure water matrix with 0.01 mol L^{-1} HCl were used as test samples for

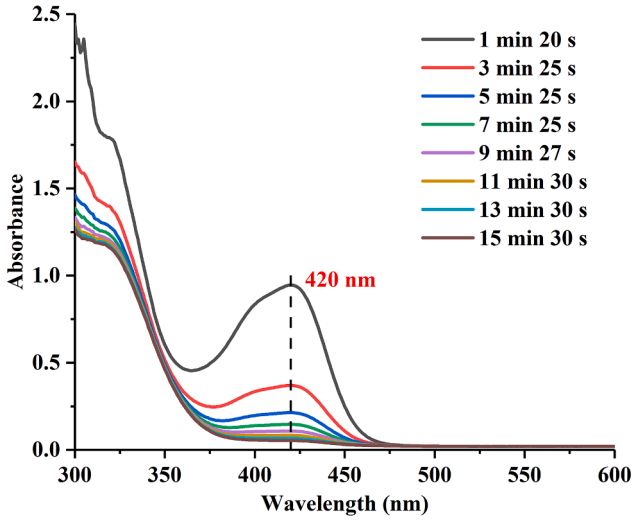

Fig. 3. Absorption spectra of the $K_3Fe(CN)_6$-GSH system in the presence of Cu (II) at different reaction times, using 15.6 nmol L^{-1} Cu(II) with a mixture of 3 mmol L^{-1} $K_3Fe(CN)_6$, 28 mmol L^{-1} GSH, and 12.5 mmol L^{-1} HAc-NaAc.

optimizing these parameters, and each sample was measured in triplicate. Results are presented as average value ± standard deviation (SD, n = 3). When optimizing one parameter, other parameters were kept constant at their optimum values.

3.2.1. Effects of reagent loop volume and reaction coil length

The effect of reagent loop (RL) volume on the reaction product signal (A_R and $\triangle A_R$) was investigated within a range of 132–442 μL (Fig. S3a). Here $\triangle A_R$ was defined as shown in Equation (2) as follows:

$$\triangle A_R = A_{R(sample)} - A_{R(blank)} \quad (2).$$

where, $A_{R(sample)}$ refers to the A_R of the sample and $A_{R(blank)}$ indicates the A_R of the blank. The $\triangle A_R$ increased in accordance with an increase in the reagent loop volume up to 353 μL, remaining almost constant from 353 μL to 442 μL. Therefore, the optimal volume of RL was set as 353 μL. Fig. S3b shows the effect of varying reaction coil length on A_R and $\triangle A_R$, from 50 to 250 cm. The $\triangle A_R$ value increased with increasing coil length, however, the blank A_R also increased accordingly. After comprehensive evaluation of the demand for method sensitivity and the suitable blank level, 200 cm was selected as the optimal reaction coil length.

3.2.2. Effect of reaction temperature

It has been well established that temperature affects catalytic reaction rates. Fig. S4 shows that the sample and blank A_R increased significantly with increasing reaction temperatures, until $\triangle A_R$ decreased slightly when the temperature exceeded 40 °C. Therefore, 40 °C was chosen as the optimal temperature.

3.2.3. Effects of HAc-NaAc buffer pH and concentration

The effect of varying HAc-NaAc buffer pH in the range of 3.8 to 5.4 on A_R and $\triangle A_R$ is illustrated in Fig. S5a. The $\triangle A_R$ reached a maximum value at a HAc-NaAc buffer pH of 4.6 and therefore, pH 4.6 was selected as the optimum buffer pH. Fig. S5b shows the effect of HAc-NaAc concentration (0.1–0.5 mol L^{-1}) on A_R and $\triangle A_R$. The $\triangle A_R$ value remained nearly steady when the HAc-NaAc buffer concentration increased to > 0.2 mol L^{-1} and as a result, 0.2 mol L^{-1} HAc-NaAc buffer was selected as the optimum concentration.

3.2.4. Effects of reagents concentration

Fig. S6a shows the effect of varying $K_3Fe(CN)_6$ concentration (0.01–0.20 mmol L^{-1}) on A_R and $\triangle A_R$. The $\triangle A_R$ significantly increased with increasing $K_3Fe(CN)_6$ concentration to 0.15 mmol L^{-1}, then remained almost constant from 0.15 to 0.20 mmol L^{-1}. Therefore, 0.15 mmol L^{-1} $K_3Fe(CN)_6$ was selected as the optimum concentration. Fig. S6b indicates the effect of varying GSH concentration (1–9 mmol L^{-1}) on A_R and $\triangle A_R$, showing that $\triangle A_R$ increased with an increase in GSH concentration. However, the A_R of blank samples also accordingly increased and after comprehensive evaluation of both the method sensitivity and GSH consumption, 9 mmol L^{-1} was chosen as the optimum GSH concentration.

3.3. Preparation of LCSW

To date, no certified copper-free seawater standard solution is available. If the seawater used to prepare standard solutions for calibration curves contains copper, an excessive matrix blank will result in the underestimation of actual Cu(II) concentrations in samples. LCSW (salinity of 35), which was obtained from the western Pacific Ocean surface utilizing a towed fish underway sampling system [42], was ultilized for the calibration of standards since its Cu(II) concentration was below the detection limit. The surface seawater was first filtered through a 0.2 μm membrane filter and then passed through tandem chelate columns, each packed with 1.0 g iminodiacetate chelating resin (Toyopearl AF-Chelate 650 M, Tosoh, Japan) to remove Cu(II). The effluent was then acidified to pH 2 using HCl to form LCSW.

3.4. Effect of carry-over

In an analytical process, the carry-over effect refers to the extent to which analytes are carried from one sample cycle to the next. To investigate the carry-over effect during Cu(II) determination, a modified version of the “Low-low–high-low” (“LLHL”) model proposed by Zhang [43] was applied. Fig. S7 shows that the effect of samples shifting from high to low concentration of Cu(II) was below the limit of detection and therefore, the effect of carry-over could be considered negligible.

3.5. Effect of salinity

To investigate the effects of varying salinity levels, LCSW was diluted with pure water at different salinities (0, 7, 14, 21, 28 and 35) to prepare calibration solutions with Cu(II) concentrations of 0, 1, 2, 5 and 10 nmol L^{-1}. The slopes and intercepts (blank A_R) of the calibration curves were calculated (Fig. S8), showing that the slope of the calibration curve increased in accordance with increasing salinity from 0 to 7, then remained almost constant when the salinity increased to > 7. In contrast, the blank A_R did not exhibit significant change only when the salinity was higher than 21. Therefore, when applying the proposed method to estuarine and coastal water analysis, it is essential to simultaneously measure salinity and correct data to account for the salinity effect. When the sample salinity is higher than 21, calibration curves established at a salinity of 35 can be used, while at a sample salinity below 21 calibration curves generated at the same salinity should be applied. In either surface or vertical waters of an open ocean where online determination is carried out, the salinity would not suddenly vary too much to be out of range limited by a selected curve, thus the curve can usually be adopted for all measurements. Even if a sudden change happens, a further data correction can be done using another calibration curve with the corresponding salinity.

3.6. Effects of interfering ions

The effect of some ions that are abundant in seawater, such as Ba^{2+}, Mg^{2+}, Ca^{2+}, Na^{+}, NH_4^{+}, NO_3^{-}, NO_3^{-}, SO_4^{2-}, Cl^{-}, on the determination of 3.8 ng mL^{-1} of Cu(II) has been investigated in the off-line catalytic kinetic determination of Cu(II) established by Prasad and Halafihi [20], and results showed that most ions did not interfere. Therefore, in this study, we focused only on the interferences of Fe(II), Fe(III), Mn, Zn, Cd,

Al, Cr, Ni, and Co ions, which may potentially interfere with the determination of Cu(II). The maximum allowable concentration of interfering ions was defined as an interference effect that reduces the recovery of Cu(II) by > 10%. In order to assesse selectivity of the method, the effect of interfering ions on the determination of 4 nmol L^{-1} Cu(II) was studied. The selected co-occurring ions and their influence on Cu(II) recovery are shown in Table S1, in which the concentration of ions applied was at least 20-fold higher than the actual concentration in seawater [44]. Results show that Cu(II) recovery ranged between 95.0% and 104%, indicating that the developed method was not affected by interference from the nine assessed co-occurring ions.

3.7. Linearity, method detection limit and repeatability

With optimal conditions, a calibration curve of Cu(II) ranging from 1 to 15 nmol L^{-1} was obtained. Typical calibrated output signals for samples prepared in an pure water matrix are shown in Fig. 4. In pure water and seawater (salinity of 35) matrices, the method detection limit (MDL) was 0.15 nmol L^{-1} and 0.23 nmol L^{-1}, respectively, which was calculated as being three-fold the standard deviation of blank samples (n = 11) divided by the slope. Cu(II) has a linear upper limit of 15 nmol L^{-1} in pure water and 10 nmol L^{-1} in seawater (salinity of 35). If the Cu (II) concentration is higher than the upper limit, the reaction coil length should be reduced. A high sample throughput rate of 26 h^{-1} was achieved, which satisfies the requirements for high spatial and temporal resolution Cu(II) determination in shipboard analysis. The repeatability of the method was evaluated using blank and 5 nmol L^{-1} Cu(II) samples, establishing RSDs of 1.52% (n = 13) and 1.10% (n = 13), respectively (Fig. S9), indicating a good level of precision. Table 1 shows the analytical characteristics of the proposed method with both pure water and seawater (salinity of 35) sample matrices, respectively. (Fig. 4).

3.8. Validation of the method

In order to evaluate the analytical applicability of the method and ensure accuracy, Cu(II) concentrations in river water and seawater were analyzed using the proposed method. As shown in Table 2, the recoveries of Cu(II) from spiked samples ranged between 95.2% and 101% (n = 3), indicating that the developed method has a high applicability.

3.9. Application

The developed underway Cu(II) analysis system was applied during a cruise in the Jiulong Estuary (China). A total of 56 measurements for Cu (II) were taken, and the distribution of surface Cu(II) concentrations is shown in Fig. 5. Cu(II) concentrations exhibited significant spatial variation, ranging from 5.37 to 17.3 nmol L^{-1}. The highest Cu(II) concentration was detected at a station located along the main channel of the Jiulong estuary near Haimen Islet, with river inputs and the influence of local anthropogenic activities likely to be responsible for the high Cu(II) concentration in this area [8,45,46]. The concentration of Cu (II) in the harbor area on the north side of the Jiulong Estuary was also higher, which may be due to fuel emissions from ships and a nearby power plant [47]. (Fig. 5).

The developed method was also applied in an on-board scenario to analyze discrete seawater samples immediately after collection from a station in the Yangtze Estuary (China). Vertical profiles of salinity, DO and Cu(II) concentrations at station Q49, are shown in Fig. 6a. The concentration of Cu(II) ranged between 4.19 nmol L^{-1} and 11.2 nmol L^{-1}. Cu(II) concentrations in the upper water layers at station Q49 exhibit a trend of estuarine mixing that decreased with increasing salinity. Furthermore, with the rapid decrease in dissolved oxygen concentration, the Cu(II) concentration exhibited a non-conservative (i.e., non-linear) behavior during the process of deoxygenation in low-oxygen level bottom water layers (Fig. 6b). This profile differs from the normal conservative behavior of Cu(II) concentrations reported in oxygenated estuary environments [8,45]. (Fig. 6).

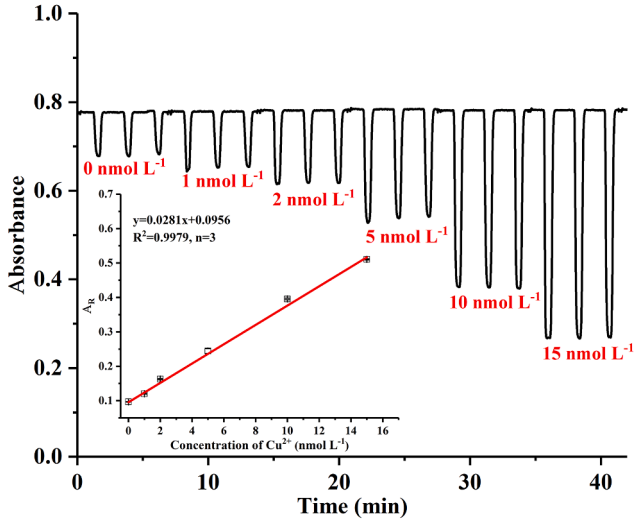

Fig. 4. Typical output signals for calibration using standard solution absorbance (n = 3). Inset shows the established calibration curve and equation.

Table 1
Analytical characteristics of the proposed method for the determination of Cu(II) in pure water and seawater (salinity = 35) matrices.

Characteristic	Pure water matrix		Seawater (S = 35) matrix	
KC length (cm)	100	200	100	200
MDL (nmol L^{-1}, n = 11)	0.24	0.15	0.51	0.23
Linear range (nmol L^{-1})	0.72–40	0.45–15	1.53–25	0.69–10
Slope of calibration curve	0.0141	0.0281	0.0233	0.0444
Linearity R^2	0.9980	0.9979	0.9958	0.9997
RSD (%, n = 13)	2.16	1.52	3.59	1.69
Sample volume (mL)	7.9			
$K_3Fe(CN)_6$ vol (mL)	2.0			
GSH volume (mL)	1.2			
HAc-NaAc volume (mL)	2.0			
Sample throughput (h^{-1})	26			

Table 2
Recovery of Cu(II) from spiked river water and seawater samples.

Sample	Salinity	Added (nmol L^{-1})	Determined (nmol L^{-1}, n = 3)	Recovery (%)
Drinking water	0	0	2.04 ± 0.21	
		4	5.98 ± 0.02	98.4 ± 0.6
River water	0	0	7.51 ± 0.03	
		5	12.6 ± 0.14	101 ± 2
Seawater 1	34	0	0.60 ± 0.06	
		3	3.58 ± 0.04	99.2 ± 1.2
Seawater 2	35	0	0.83 ± 0.07	
		5	5.59 ± 0.01	95.2 ± 0.2

4. Conclusions

In summary, the study established a sensitive and automated method of rFIA-LWCC combined with catalytic kinetic spectrophotometric detection for the determination of Cu(II) in estuarine and coastal waters. The proposed method has the advantages of low method detection limit, high automation and precision, rapid sample throughput, wide linear range, and low reagent and sample consumption requirements. The effect of interference due to carry-over and the presence of nine commonly coexisting ions, were found to be negligible. The effect of salinity was well investigated, showing that accurate Cu(II) concentration determination requires calibration to be performed at a corresponding salinity.

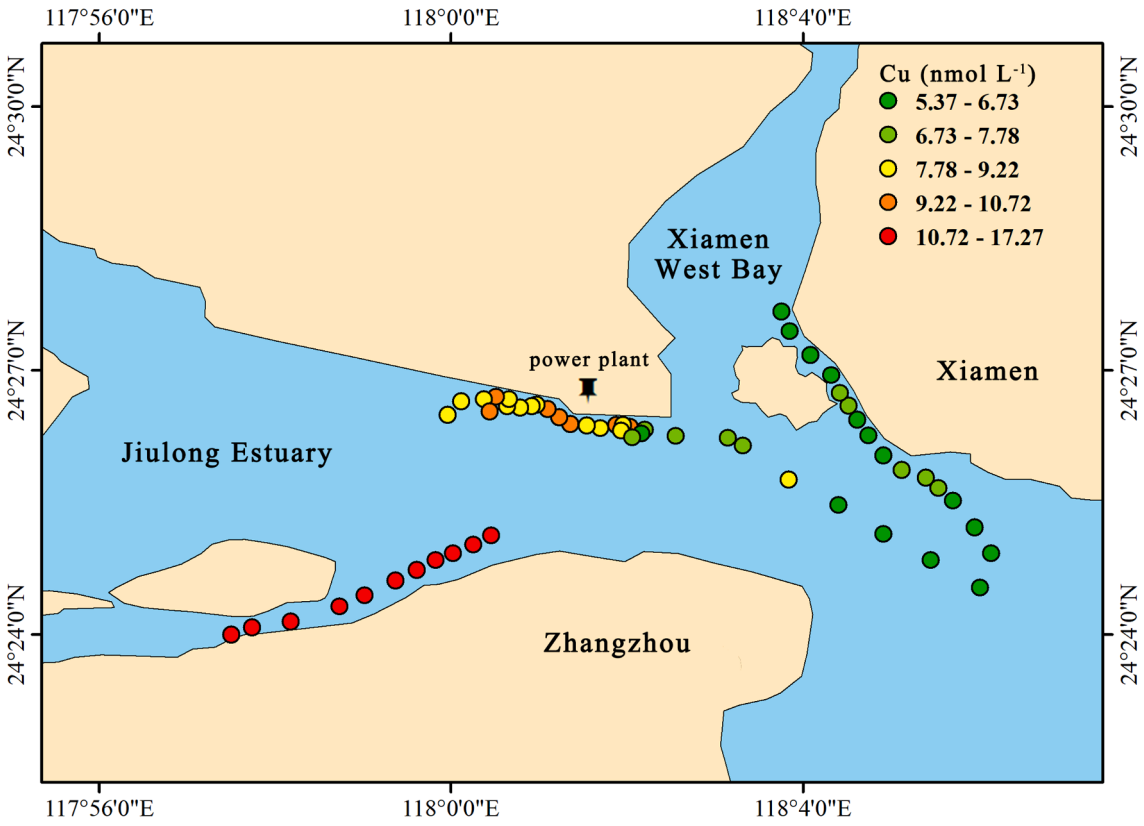

Fig. 5. Distribution of Cu(II) in the Jiulong Estuary (China) on 26th June 2021.

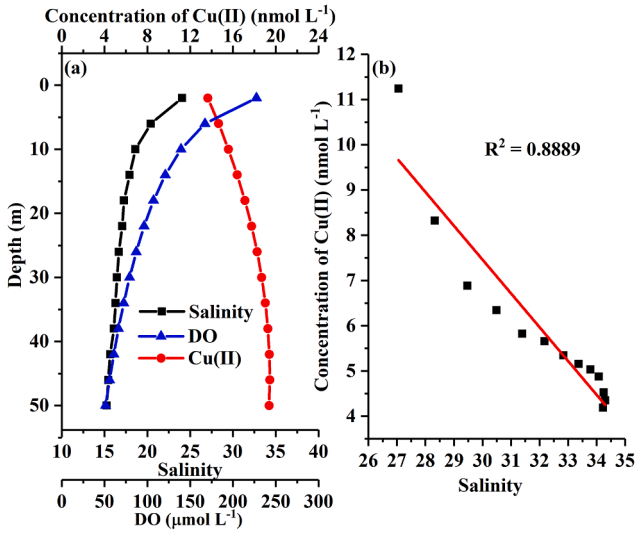

Fig. 6. Vertical profiles of (a) salinity, DO and Cu(II) concentrations at sampling station Q49, in the Yangtze Estuary (China); and (b) the non-conservative relationship between Cu(II) concentration and salinity, across a low oxygen profile.

Underway on-line analysis of Cu(II) concentrations in surface seawater of the Jiulong Estuary (China) and on-board analysis of discrete samples in the Yangtze Estuary (China) and were successfully carried out using the porposed method. Considering that the MDL is three-fold higher than the minimum detection limit (0.5 nmol L^{-1} [48]), this method can effectively be applied to underway or on-board analysis of Cu(II) geochemistry in environments ranging from estuaries to the open ocean, such as in the international GEOTRACES program [49].

Declaration of Competing Interest

The authors declare that they have no known competing financial interests or personal relationships that could have appeared to influence the work reported in this paper.

Acknowledgements

This work was supported by the National Natural Science Foundation of China (41876083). We are particularly grateful to the Project of Long-term Observation and Research Plan in the Changjiang Estuary and Adjacent East China Sea (LORCE) of the Second Institute of Oceanography, Ministry of Natural Resources for providing the unpublished data on salinity and dissolved oxygen, as well as to Mr. Jiayi Jiang of the College of the Environment and Ecology, Xiamen University, for help in sampling. We also thank the staff of the research vessels Runjiang I and Haiyang II, for their assistance.

Appendix A. Supplementary data

Supplementary data to this article can be found online at https://doi.org/10.1016/j.microc.2022.107441.

References

[1] W.G. Sunda, Feedback interactions between trace metal nutrients and phytoplankton in the ocean, Front. Microbiol. 3 (2012) 1–22, https://doi.org/10.3389/fmicb.2012.00204.
[2] A.L. Annett, S. Lapi, T.J. Ruth, M.T. Maldonado, The effects of Cu and Fe availability on the growth and Cu: C ratios of marine diatoms, Limnol. Oceanogr. 53 (2008) 2451–2461, https://doi.org/10.2307/40058335.
[3] J.W. Moffett, R.G. Zika, Measurement of copper(I) in surface waters of the subtropical Atlantic and Gulf of Mexico, Geochim. Cosmochim. Acta 52 (1988) 1849–1857, https://doi.org/10.1016/0016-7037(88)90008-7.

[4] M. Gledhill, M. Nimmo, S.J. Hill, M.T. Brown, The toxicity of copper(II) species to marine algae, with particular reference to macroalgae, J. Phycol. 33 (1997) 2–11, https://doi.org/10.1111/j.0022-3646.1997.00002.x.

[5] B.M. Sanders, K.D. Jenkins, W.G. Sunda, J.D. Costlow, Free cupric ion activity in seawater: effects on metallothionein and growth in crab larvae, Science 222 (1983) 53–55, https://doi.org/10.1126/science.222.4619.53.

[6] R.W. Andrew, K.E. Biesinger, G.E. Glass, Effects of inorganic complexing on the toxicity of copper to daphnia magna, Water Res. 11 (1977) 309–315, https://doi.org/10.1016/0043-1354(77)90064-1.

[7] C.A. Flemming, J.T. Trevors, Copper toxicity and chemistry in the environment: a review, Water, Air, and Soil Pollution 44 (1-2) (1989) 143–158.

[8] A.P. Hollister, H. Whitby, M. Seidel, P. Lodeiro, M. Gledhill, A. Koschinsky, Dissolved concentrations and organic speciation of copper in the Amazon River estuary and mixing plume, Mar. Chem. 234 (2021) 104005.

[9] A. Lopez Garcia, E. Blanco Gonzalez, A. Sanz-Medel, Determination of trace elements in seawater by electrothermal atomic absorption spectrometry with and without a preconcentration step, Microchim. Acta 112 (1-4) (1993) 19–29.

[10] Z. Liu, S. Huang, Determination of copper and cadmium in sea water by preconcentration and electrothermal atomic absorption spectrometry, Anal. Chim. Acta 267 (1992) 31–37, https://doi.org/10.1016/0003-2670(92)85003-O.

[11] O. Aydin Urucu, A. Aydin, Coprecipitation for the determination of copper(II), zinc (II), and lead(II) in seawater by flame atomic absorption spectrometry, Anal. Lett. 48 (2015) 1767–1776, https://doi.org/10.1080/00032719.2014.999275.

[12] C. Karadas, D. Kara, Dispersive liquid-liquid microextraction based on solidification of floating organic drop for preconcentration and determination of trace amounts of copper by flame atomic absorption spectrometry, Food Chem. 220 (2017) 242–248, https://doi.org/10.1016/j.foodchem.2016.09.005.

[13] Z. Li, J. Li, Y. Wang, Y. Wei, Synthesis and application of surface-imprinted activated carbon sorbent for solid-phase extraction and determination of copper (II), Spectro. Acta Pt. A-Molec. Biomolec. Spectr. 117 (2014) 422–427, https://doi.org/10.1016/j.saa.2013.08.045.

[14] A. Milne, W. Landing, M. Bizimis, P. Morton, Determination of Mn, Fe Co, Ni, Cu, Zn, Cd and Pb in seawater using high resolution magnetic sector inductively coupled mass spectrometry (HR-ICP-MS), Anal. Chim. Acta 665 (2010) 200–207, https://doi.org/10.1016/j.aca.2010.03.027.

[15] F. Quéroué, A. Townsend, P. van der Merwe, D. Lannuzel, G. Sarthou, E. Bucciarelli, A. Bowie, Advances in the offline trace metal extraction of Mn Co, Ni, Cu, Cd, and Pb from open ocean seawater samples with determination by sector field ICP-MS analysis, Anal. Methods 6 (9) (2014) 2837–2847.

[16] K.H. Coale, K.S. Johnson, P.M. Stout, C.M. Sakamoto, Determination of copper in sea water using a flow-injection method with chemiluminescence detection, Anal. Chim. Acta 266 (1992) 345–351, https://doi.org/10.1016/0003-2670(92)85062-B.

[17] D. Axel, C. Zanna, R. Tomas, Q. Fabien, Microplate-reader method for the rapid analysis of copper in natural waters with chemiluminescence detection, Front. Microbiol. 3 (2012) 437, https://doi.org/10.3389/fmicb.2012.00437.

[18] C.E. Holm, Z. Chase, H.W. Jannasch, K.S. Johnson, Development and initial deployments of an autonomous in situ instrument for long-term monitoring of copper (II) in the marine environment, Limnol. Oceanogr. Meth. 6 (7) (2008) 336–346.

[19] X. Yu, Q. Wang, The determination of copper ions based on sensitized chemiluminescence of silver nanoclusters, Microchim. Acta 173 (2011) 293–298, https://doi.org/10.1007/s00604-011-0549-8.

[20] S. Prasad, T. Halafihi, Development and validation of catalytic kinetic spectrophotometric method for determination of copper(II), Microchim. Acta 142 (2003) 237–244, https://doi.org/10.1007/s00604-003-0023-3.

[21] H.S. Zhang, L. Liu, H.W. Ji, Mechanistic study and kinetic determination of Cu(II) by the catalytic kinetic spectrophotometric method, J Ocean U China 18 (2019) 144–150, https://doi.org/10.1007/s11802-019-3592-4.

[22] M. Andres, M.L. Marina, S. Vera, Spectrophotometric determination of copper(II), nickel(II) and cobalt(II) as complexes with sodium diethyldithiocarbamate in cationic micellar medium of hexadecyltrimethylammonium salts, Talanta 41 (1994) 179–185, https://doi.org/10.1016/0039-9140(94)80105-3.

[23] M.R. Callahan, E.A. Kaltenbacher, R.H. Byrne, In-situ measurements of Cu in an estuarine environment using a portable spectrophotometric analysis system, Environ. Sci. Technol. 38 (2004) 587–593, https://doi.org/10.1021/es034538r.

[24] M. Hiraide, H. Hommi, H. Kawaguchi, Diethyldithiocarbamate (DDTC) extraction of copper(II) and iron(III) associated with humic substances in water, Fresenius J. Anal. Chem. 342 (1992) 387–390, https://doi.org/10.1007/BF00322191.

[25] S. Prasad, Kinetic method for determination of nanogram amounts of copper(II) by its catalytic effect on hexacynoferrate(III)-citric acid indicator reaction, Anal. Chim. Acta 540 (2005) 173–180, https://doi.org/10.1016/j.aca.2005.03.011.

[26] J.M. Jurado, M.J. Martin, F. Pablos, A. Moreda-Pineiro, P. Bermejo-Barrera, Direct determination of copper, lead and cadmium in aniseed spirits by electrothermal atomic absorption spectrometry, Food Chem. 101 (2007) 1296–1304, https://doi.org/10.1016/j.foodchem.2006.01.027.

[27] M.N. Uddin, M.A. Salam, M.A. Hossain, Spectrophotometric measurement of Cu (DDTC)2 for the simultaneous determination of zinc and copper, Chemosphere 90 (2013) 366–373, https://doi.org/10.1016/j.chemosphere.2012.07.029.

[28] P.J. Worsfold, R. Clough, M.C. Lohan, P. Monbet, P.S. Ellis, C.R. Quetel, G.H. Floor, I.D. McKelvie, Flow injection analysis as a tool for enhancing oceanographic nutrient measurements-a review, Anal. Chim. Acta 803 (2013) 15–40, https://doi.org/10.1016/j.aca.2013.06.015.

[29] J. Ruzicka, From continuous flow analysis to programmable flow injection techniques, A history and tutorial of emerging methodologies, Talanta 158 (2016) 299–305, https://doi.org/10.1016/j.talanta.2016.05.070.

[30] F.R. Mansour, N.D. Danielson, Reverse flow-injection analysis, Trac-Trends, Anal. Chem. 40 (2012) 1–14, https://doi.org/10.1016/j.trac.2012.06.006.

[31] K. Lin, P. Li, Q. Wu, S. Feng, J. Ma, D. Yuan, Automated determination of ammonium in natural waters with reverse flow injection analysis based on the indophenol blue method with o-phenylphenol, Microchem. J. 138 (2018) 519–525.

[32] K. Lin, L. Wang, J. Xu, S. Huang, H. Guo, Y. Huo, Y. Zhang, Reverse flow injection method for field determination of nitrate in estuarine and coastal waters using a custom-made linear light path flow cell and the vanadium reduction method, Microchem. J. 172 (2021), 106901, https://doi.org/10.1016/j.microc.2021.106901.

[33] A. Dias, E.P. Borges, E. Zagatto, P.J. Worsfold, A critical examination of the components of the Schlieren effect in flow analysis, Talanta 68 (2006) 1076–1082, https://doi.org/10.1016/j.talanta.2005.06.071.

[34] R. Páscoa, I. Tóth, A. Rangel, Review on recent applications of the liquid waveguide capillary cell in flow based analysis techniques to enhance the sensitivity of spectroscopic detection methods, Anal. Chim. Acta 739 (2012) 1–13, https://doi.org/10.1016/j.aca.2012.05.058.

[35] G.H. Chen, D.X. Yuan, Y.M. Huang, M. Zhang, M. Bergman, In-field determination of nanomolar nitrite in seawater using a sequential injection technique combined with solid phase enrichment and colorimetric detection, Anal. Chim. Acta 620 (2008) 82–88, https://doi.org/10.1016/j.aca.2008.05.019.

[36] Y. Zhu, D.X. Yuan, Y.M. Huang, J. Ma, S.C. Feng, A sensitive flow-batch system for on board determination of ultra-trace ammonium in seawater: method development and shipboard application, Anal. Chim. Acta 794 (2013) 47–54, https://doi.org/10.1016/j.aca.2013.08.009.

[37] T. Wang, Y.M. Huang, J. Xu, W.D. Guo, Y. Zhu, D.X. Yuan, A modified method of on-line solid phase extraction and fluorometric detection for underway monitoring and onboard analysis of trace ammonium in seawater, Deep-Sea Res. Part I-Oceanogr. Res. Pap. 173 (2021), 103547, https://doi.org/10.1016/j.dsr.2021.103547.

[38] L.J. Gimbert, P.J. Worsfold, Environmental applications of liquid-waveguide-capillary cells coupled with spectroscopic detection, Trac-Trends, Anal. Chem. 26 (2007) 914–930, https://doi.org/10.1016/j.trac.2007.08.005.

[39] T. Wang, Y. Huang, J. Xu, W. Guo, D. Yuan, Development and application of a shipboard method for spectrophotometric determination of nanomolar dissolved sulfide in estuarine surface waters using reverse flow injection analysis coupled with a long path length liquid waveguide capillary cell, Microchem. J. 168 (2021), 106522, https://doi.org/10.1016/j.microc.2021.106522.

[40] J. Yu, C. Zhang, D. Ping, C. Dong, Determination of trace copper in natural waters using flow injection chemiluminescence system with on-line solid phase extraction, IEEE (2009), https://doi.org/10.1109/ICBBE.2009.5162631.

[41] E.P. Achterberg, T.W. Holland, A.R. Bowie, R. Mantoura, P.J. Worsfold, Determination of iron in seawater, Anal. Chim. Acta 442 (2001) 1–14, https://doi.org/10.1016/S0003-2670(01)01091-1.

[42] Y.M. Huang, D.X. Yuan, Y. Zhu, S.C. Feng, Real-time redox speciation of iron in estuarine and coastal surface waters, Environ. Sci. Technol. 49 (2015) 3619–3627, https://doi.org/10.1021/es505138f.

[43] J.Z. Zhang, Distinction and quantification of carry-over and sample interaction in gas segmented continuous flow analysis, J. Autom. Chem. 19 (1997) 205–212, https://doi.org/10.1155/S1463924697000254.

[44] K.W. Bruland, R. Middag, M.C. Lohan, Controls of trace metals in seawater, Treat. Geochem. (Second Ed.) 8 (2014) 19–51.

[45] B. Grant, E.A. Boyle, S.S. Huested, The chemical mass balance of the amazon plume-II. Copper, nickel, and cadmium, Deep-Sea Res, Part I-Oceanogr. Res. Pap. 29 (1982) 1355–1364, https://doi.org/10.1016/0198-0149(82)90013-9.

[46] A. Cobelo-Garcia, R. Prego, Land inputs, behaviour and contamination levels of copper in a ria estuary (NW Spain), Mar. Environ. Res. 56 (2003) 403–422, https://doi.org/10.1016/S0141-1136(03)00002-3.

[47] L. Wang, J.H. Qi, J.H. Shi, X.J. Chen, H.W. Gao, Source apportionment of particulate pollutants in the atmosphere over the Northern Yellow Sea, Atmos. Environ. 70 (2013) 425–434, https://doi.org/10.1016/j.atmosenv.2012.12.041.

[48] R. Saeed, J. Wu, Dissolved and colloidal copper in the tropical South Pacific, Geochim. Cosmochim. Acta 233 (2018) 81–94, https://doi.org/10.1016/j.gca.2018.05.008.

[49] S. Roshan, J.F. Wu, The distribution of dissolved copper in the tropical-subtropical north Atlantic across the GEOTRACES GA03 transect, Mar. Chem. 176 (2015) 189–198, https://doi.org/10.1016/j.marchem.2015.09.006.